Reaction and microstructure of metakaolin-based geopolymer

Haruki Nakashima[a], Kiyofumi Kurumisawa[b]*

a: Division of Sustainable Resources Engineering, Graduate School of Engineering, Hokkaido University, Japan

b: Division of Sustainable Resources Engineering, Faculty of Engineering, Hokkaido University, Japan

*: Corresponding author, kurumi@eng.hokudai.ac.jp

A B S T R A C T

The reaction mechanism of geopolymers remains unclear, yet it significantly influences their early-age properties such as strength and microstructure. In this study, the heat of reaction and compressive strength were measured for geopolymers with varying SiO_2/Al_2O_3 and H_2O/Al_2O_3 ratios. Results showed that increasing both ratios decreased the degree of reaction and the peak heat flow, likely due to reduced alkalinity and hindered dehydration during polymerization. A certain degree of reaction is essential for strength development, while unreacted metakaolin can act as a filler, contributing positively to strength. An increased H_2O/Al_2O_3 ratio initially enhances workability and strength, but excessive water leads to higher porosity and reduced strength. Based on the balance between reactivity and porosity, the optimal mix proportions were found to be SiO_2/Al_2O_3 = 3.5–3.75 and H_2O/Al_2O_3 = 11 for K-based geopolymers, and SiO_2/Al_2O_3 = 3.75 with H_2O/Al_2O_3 = 11–12 for Na-based geopolymers.

Keywords: Geopolymer; Metakaolin; Alkali activator; Strength development; Pore structure

1. Introduction

Cement production leads to the emission of significant amounts of CO_2, which causes global warming [1,2]. Therefore, cement production needs to be limited to minimize CO_2 emissions, and alternative materials are required. Geopolymers are an alternative material to cement and are manufactured through the reaction of an alkaline activator and precursors, such as metakaolin, fly ash, and blast-furnace slag [3,4]. A 60% reduction in CO_2 emissions is possible if geopolymers are produced with the same strength as cement concrete [5]. Geopolymers have advantages, such as good fire resistance and good acid resistance, enabling materials to be used for extended periods and reducing energy consumption [6-10]. In addition, geopolymers exhibit adsorption and are useful for disposing of radioactive materials and fixing heavy metals [11,12]. However, geopolymers have drawbacks for practical applications, such as cracking caused by shrinkage and efflorescence, high material cost, and production under high pH [13-15]. In particular, the reaction mechanism of geopolymers is unclear. Geopolymers are synthesized from several precursors and an alkaline activator. Precursors such as fly ash, blast-furnace, and metakaolin exhibit different characteristics, such as chemical properties, mineral composition, and particle shape. NaOH, KOH, Na_2SiO_3, and K_2SiO_3 in the form of alkaline solutions are generally used for geopolymers. Geopolymers are synthesized through various reactions and yield different products, mainly N(or K)-A-S-H and C(-A)-S-H. Furthermore, geopolymers can be tailored for various functions based on the intended use, and hence, a clear understanding of their

reactions is required. The use of metakaolin as a precursor is suitable for analyzing reaction mechanisms because metakaolin does not contain calcium and produces C(-A)-S-H. By clarifying the reaction of a simple system, the reaction of a more complex system can be revealed. However, studies on metakaolin geopolymers have not been conducted extensively compared to those on other geopolymers [16]. Moreover, metakaolin is known for its relatively stable chemical composition and high reactivity, and when geopolymers are produced using MK with a certain reactivity, the products and mechanical properties are controlled by the alkaline activator [17]. In conclusion, the reaction in metakaolin-based geopolymers can be controlled by controlling the alkaline activator mixture.

Analyzing the reaction kinetics of geopolymers helps reveal the reactions in geopolymers. The heat of reaction can be measured continuously, and the progress of the reaction can be observed [18,19]. It is easier to develop heat evolution and cumulative heat using metakaolin than using fly ash or blast-furnace slag as precursors of geopolymers because metakaolin exhibits a higher chemical activity than fly ash and blast-furnace slag. The solid/liquid (S/L) ratio does not significantly influence heat evolution and cumulative heat; however, as the concentration of the alkali activator or curing temperature increases, the first heat evolution peak and cumulative heat increases [18,19].

The reaction between precursors and alkali activator can also be determined from the setting time. Dupuy et al. examined the reaction of metakaolin with potassium or potassium + sodium-based alkali activators and continuously measured the viscosity values until setting [20]. They found that an ideal Si/M ratio (M = K or K+Na) exists with low initial viscosity and gradually increasing viscosity. Reducing the S/L ratio resulted in a low viscosity and longer setting time; however, a weak network was generated, possibly because of the low water content and slow dissolution of metakaolin.

The microstructures of geopolymers formed as a result of the reaction have also been examined. Lizcano et al. captured scanning electron microscopy (SEM) images of metakaolin geopolymer after 1 day and observed that the structure changed with the alkali species and Si/Al ratio of the alkaline activator [21]. The K-based geopolymer had a less porous and more homogeneous structure than the Na-based geopolymer. Geopolymers with Si/Al ratios of 1.5 and 2.0 had a denser and more homogeneous structure than those with an Si/Al ratio of 1.25. Rovnanik measured the cumulative and differential pore volumes of geopolymers after 1, 3, 7, and 28 days to assess the changes in the microstructure and pores [22]. When the reaction occurred rapidly owing to the increased curing temperature, the pore volume and pore size increased. In general, compressive strength increases with increasing temperature [23], elevated temperatures increase pore volume and differential pore volume and decreases strength [22]. Therefore, an optimum value is required for the curing temperature, as very high and very low temperatures degrade the performance of geopolymers. Chen et al. determined the optimum mixing conditions for metakaolin-based geopolymers and found that the best condition for curing was 60 °C for 7 days, at which the geopolymers exhibited the highest compressive strength [24].

Researchers have found that strength is influenced by other parameters other than temperature. As the alkali activator concentration increases, the pH and strength of geopolymers increase [19]. Strength also increases with the Si/Al ratio [25].

Duxson et al. reported that the compressive strength at 7 and 28 days is constant regardless of the Si/Al ratio and alkali species [25]. In particular, uniaxial compression test results have shown that when cured at room temperature, the strength at 3 days is close to 80% of that at 28 days. These findings suggest that the reaction and microstructure formation up to 3 days determines the compressive

strength development. This trend applies not only to strength development but also to other mechanical properties. The authors have also investigated the improvement of flowability and diffusion performance of geopolymers [26,27]. Factors that determine properties (such as compressive strength, shrinkage, and permeability) include the strength of the reacted product and the pore structure.

The aim of this study was to examine the reaction of metakaolin-based geopolymers up to 3 days of curing and analyze the effect of mixing conditions on the reaction to reveal the reaction mechanism of geopolymers. We investigated the initial reaction of metakaolin-based geopolymers using isothermal calorimetry, ultrasonic pulse velocity (UPV) test, and uniaxial compression test. Isothermal calorimetry indicates the reaction rate based on the measured heat flow. UPV tests determine the ratio of solid parts bonded together, and uniaxial compression tests are typically used to evaluate the mechanical properties of materials. Finally, the influence of porosity structure on strength development was clarified.

2. Experimental

2.1 Materials and preparation of samples

The metakaolin (Metamax, BASF, Rheinland-Pfalz, Germany) used in this study was an aluminosilicate powder for sourcing alumina and silica (SiO_2/Al_2O_3 = 2.0 in mol/mol). The chemical composition and particle size distribution of the metakaolin are presented in Table 1 and Fig. 1, respectively. The average particle size and the Brunauer–Emmett–Teller (BET) specific surface area were 1.3 μm and 12.9 $m^2 \cdot g^{-1}$, respectively. X-ray diffraction (XRD) measurements performed using an internal standard (corundum) indicated that most of the metakaolin was amorphous. The alkali activators were prepared using potassium silicate solution (Fujifilm Wako Pure Chemical Co., Osaka, Japan), sodium silicate solution (Fujifilm Wako Pure Chemical Co., Osaka, Japan), potassium hydroxide (Kanto Chemical Co., Inc., Tokyo, Japan), and sodium hydroxide (Kanto Chemical Co., Inc., Tokyo, Japan) as reagent grades, and purified water that had a conductivity lower than 0.1 mS/m. The alkali activators were mixed with chemicals at least 24 h prior to geopolymer preparation. Alkaline solutions were prepared using sodium silicate (Na_2SiO_3), sodium hydroxide (NaOH), potassium silicate (K_2SiO_3), potassium hydroxide (KOH), and purified water. The SiO_2/Na_2O ratio of sodium silicate was 2.176, and the SiO_2/K_2O ratio of potassium silicate was 2.012. NaOH and KOH had purity values higher than 98% and 87%, respectively.

Samples were named based on their alkali species, SiO_2/Al_2O_3 molar ratio, and H_2O/Al_2O_3 molar ratio. The molar of SiO_2 and H_2O indicates the molar in the alkali activator, whereas the molar of Al_2O_3 represents the molar in metakaolin. For example, in N1.5S11, “N” indicates that sodium is the alkali species in the alkali activator. “1.5S” indicates that the alkali activator is prepared using SiO_2/Al_2O_3 = 1.5. “11” indicates that the alkali activator is prepared using H_2O/Al_2O_3 = 11. In the case of KS9, “K” indicates that the alkali species in the alkali activator is potassium. “S” indicates that the alkali activator is prepared using SiO_2/Al_2O_3 = 1.0, where 1.0 is excluded. “9” indicates that the alkali activator is prepared using H_2O/Al_2O_3 = 9. The mix proportions of the geopolymers are summarized in Table 2.

These mix proportions are similar to that of Duxson et al. [25]. The range of Si/Al adopted in this study was set with reference to the result that compressive strength was maximum at Si/Al = 1.9 in Ref. [22]. Also, M. F. Oliveira et al. investigated optimal mix design in terms of workability and efflorescence [28]; the mix design of this study was close to that of their study and yielded good results.

The flowchart of the geopolymer preparation is shown in Fig. 2. For mortar sample production, after mixing metakaolin and fine aggregate for 1 min at a low speed, the activator was first added to the mixer and stirred for 5 min at a low speed. It was then stirred for 1 min manually and finally stirred for 10 min at a high speed. Next, the fresh samples were poured into a plastic mold and cured at 20 ℃. In the small-angle X-ray scattering (SAXS), SEM, and transmission electron microscopy (TEM) analyses, the samples were freeze-dried with liquid nitrogen and examined.

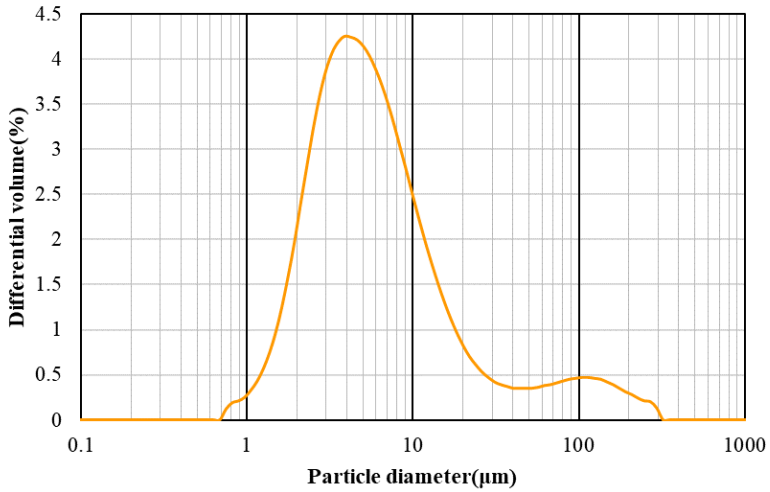

Fig. 1 Particle size distribution of metakaolin

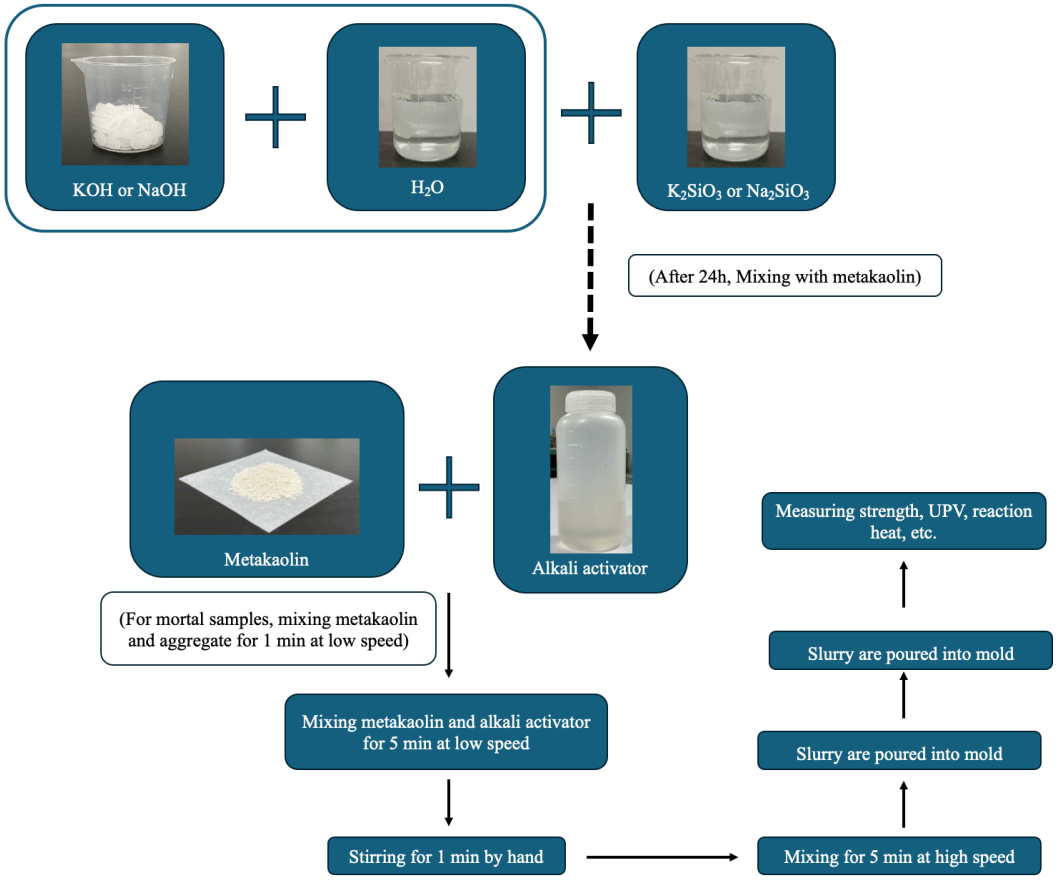

Fig. 2 Flowchart showing the preparation of geopolymer

Table 1 Chemical composition of metakaolin (wt%)

SiO_2	Al_2O_3	Fe_2O_3	Na_2O	K_2O	CaO
52.78	45.37	0.35	0.22	0.12	0.020

Table 2 Mix proportions of specimens

Sample	Composition of sample	M_2O/Al_2O_3	*m*: SiO_2/Al_2O_3	*n*: H_2O/Al_2O_3
KS11	$K_2O \cdot Al_2O_3 \cdot mSiO_2 \cdot nH_2O$	1.0	3.0	11.0
K1.5S11		1.0	3.5	
K1.75S11		1.0	3.75	
KS9		1.0	3.0	9.0
NS11	$Na_2O \cdot Al_2O_3 \cdot mSiO_2 \cdot nH_2O$	1.0	3.0	11.0
N1.5S11		1.0	3.5	
N1.75S11		1.0	3.75	
NS12		1.0	3.0	12.0
NS15		1.0		15.0

2.2 Experimental methods

(1) Viscosity measurement

The viscosities of alkali activators were measured using a B-type viscometer (DV2T, Eko Instruments Co., Ltd., Tokyo, Japan). The spindle was connected to the spring, which measured the torque generated via flow resistance when the spindle was rotated in the solution. The error of the measured value was within ±5 mPa·s.

(2) Flow test

For the flow test, the samples were first poured into a cylindrical mold (diameter: 50 mm; height: 50 mm) after mixing. The mold was lifted up, and the diameter of the samples were recorded as the flow value (mm).

(3) pH test

The pH values of the alkali activators were measured using a pH meter (D-51, Horiba, Ltd., Kyoto, Japan). Prior to pH measurements, calibration was performed using a pH standard solution. The pH values were measured when the potential and temperature change for 10 s were ±1 mV and ±2 ℃, respectively.

(4) Uniaxial compressive test

Cylindrical specimens (Φ 50 mm × 100 mm) were used for the compressive strength test. The uniaxial compressive strength was determined using an automatic compression tester (Hi-ACTIS-2000, Marui & Co., Ltd., Osaka, Japan). The maximum stress during the test, determined from the breaking point of each specimen, was divided by the cross-sectional area of the end face to obtained the uniaxial compressive strength. The test was repeated using three specimens for each activator, and the average value was adopted as the compressive strength.

(5) UPV test

UPV was measured using an ultrasonic nondestructive tester (UST MIN-020-1-00, Marui & Co., Ltd., Osaka, Japan). Samples were blended in the mortar mixer and poured into molds, each with a length and width of 50 mm and height of 100 mm. Polyethylene film was wrapped at the top of the mold to prevent water evaporation. The mold had holes on each side, into which the ultrasonic transmitter and receiver were attached. Ultrasonic waves were transmitted from the transmitter to the receiver, and the time was measured. The UPV value was calculated by dividing the transmission time by 50 mm.

(6) Isothermal calorimetry

Heat flow was monitored using a isothermal calorimeter (MMC-5116, Tokyo Ricoh Co., Ltd.), measured at 20 °C for 7 days. Samples were blended by hand outside the calorimeter and immediately placed in the calorimeter. Therefore, the result was unstable until after 1 h.

(7) Mercury intrusion porosimetry (MIP)

Immediately the geopolymer paste reached a specified age, it was roughly crushed to particle sizes of 2.5–5 mm using a hammer. The reaction was stopped using liquid nitrogen and a freeze dryer. Subsequently, the pore-size distribution was determined using MIP (AutoPore V 9620, Micromeritics Instrument Co., Georgia, USA). The measurement range of the pore size was 3–400 μm. A 1.0 g sample was used for the measurement, and this amount is sufficient for measurement reproducibility.

(8) Nitrogen adsorption (NAD)

Each sample was crushed in a ball mill, and the powder was utilized for the NAD analysis. Prior to measurements, vacuum drying was performed at room temperature for 24 h. The specific surface area and pore structure of the sample were determined via NAD measurements (BELSORP Max, MicrotracBEL CO., Osaka, Japan). The sample was approximately 0.2 g. The BET specific surface area was calculated from the NAD measurements, and pore size distribution was determined using the Barrett–Joyner–Halenda method.

(9) SAXS measurements

SAXS and wide-angle X-ray scattering (Nano-inXider, Xenocs, Grenoble, France) were adopted for pore measurements. X-rays from a Cu source (λ = 1.54 Å, 50 kV, 0.6 mA) were scattered by the sample and recorded using a detector. Powders were placed between Kapton windows in a 0.5 mm Al washer without being compressed. The sample environment was vacuumed. A Guinier Porod model was used for calculations, and based on the assumption of spherical pores (slope q_0), polydispersity was neglected.

(10) SEM and energy dispersive X-ray (EDX) analysis

A scanning electron microscope (JSM-IT200, Jeol Ltd., Tokyo, Japan) was used to characterize the microstructures of the samples. For SEM observations, the crushed samples were embedded in epoxy resin, and a cross-section with a polished surface was observed. Platinum sputtering was used to make the surface electrically conductive. The procedure was performed at an accelerating voltage of 15 keV and a working distance of 10 mm. In addition, EDX point analysis was performed to determine the

elemental composition of the product in the geopolymers. In the point analysis, 10 or more points were analyzed using the ZAF method, and the average value was calculated.

(11) TEM measurements

The powder sample was dispersed on a Cu grid, and TEM (Titan G2 60-300) was performed at 60 kV.

(12) High-energy X-ray diffraction (HEXD)

HEXD data were analyzed at SPring-8 (BL04B2 beam-line) using a two-axis diffractometer. The incident X-ray energy was 61.5 keV, and the diffraction patterns were detected by four CdTe and three Ge detectors. A vacuum chamber was used to prevent air scattering around the sample. The powder sample was filled into a capillary tube. The total correlation function, T(r), calculated by a previous study [26] was used.

3. Results and discussion

3.1 Viscosity, pH of alkali activators, and flow test of geopolymer

The viscosities of the alkali activators are presented in Fig. 3. When the SiO_2/Al_2O_3 and H_2O/Al_2O_3 ratios were the same, the K-based solutions had a lower viscosity than the Na-based solutions. In addition, the viscosity increased with increasing SiO_2/Al_2O_3 ratio or decreasing H_2O/Al_2O_3 ratio, which was particularly significant for Na-based solutions. The viscosity values of potassium silicate (K_2SiO_3) and sodium silicate (Na_2SiO_3) used as raw materials were also measured. These values are close to them of K1.75S11 or N1.75S11.

The pH values of different alkali activators are presented in Fig. 4. The pH values of potassium silicate and sodium silicate were also measured. However, these values were lower than those of the alkali activators because the alkali activators were prepared by adding KOH or NaOH to the silicate solution. The K-based solutions had higher pH values than the Na-based solutions at the same SiO_2/Al_2O_3 and H_2O/Al_2O_3 ratios. Additionally, increasing the SiO_2/Al_2O_3 or H_2O/Al_2O_3 ratio resulted in low pH values. This result was identical to that of Jansson et al. They found that samples with higher SiO_2/Na_2O ratios yielded lower pH values and delayed setting [30]. In this study, the M_2O/ Al_2O_3 ratio was fixed to 1.0 for all specimens, thus ensuring that the SiO_2/Na_2O ratio was the same as the SiO_2/Al_2O_3 ratio. However, the pH meter used in this study had a range of 0–14, and the pH values were only used for reference. Gharzouni et al. measured the pH values of a metakaolin-based geopolymer, which ranged from 10 to 14 [17]. It would be expected that the pH of the alkali activator would decrease with the addition of the precursor.

The flow values of the specimens are presented in Fig. 5. The flow decreased with increasing SiO_2/Al_2O_3 ratio in all the samples. For the Na-based samples, the flow value increased as the H_2O/Al_2O_3 ratio decreased. When the SiO_2/Al_2O_3 and H_2O/Al_2O_3 ratios were the same, the K-based samples yielded higher flow values than the Na-based samples owing to differences in the charge/radius ratio and hydration energy of alkali cation [31]. Na^+ requires higher hydration energy than K^+ because Na^+ has a smaller ion radius than K^+. Therefore, K^+ interacts more with water, and the K-based geopolymer yielded a higher flow value. A good correlation was observed between solution viscosity and flow. Therefore, the mixing design influences the workability and pH of specimens, which influence the reaction rate.

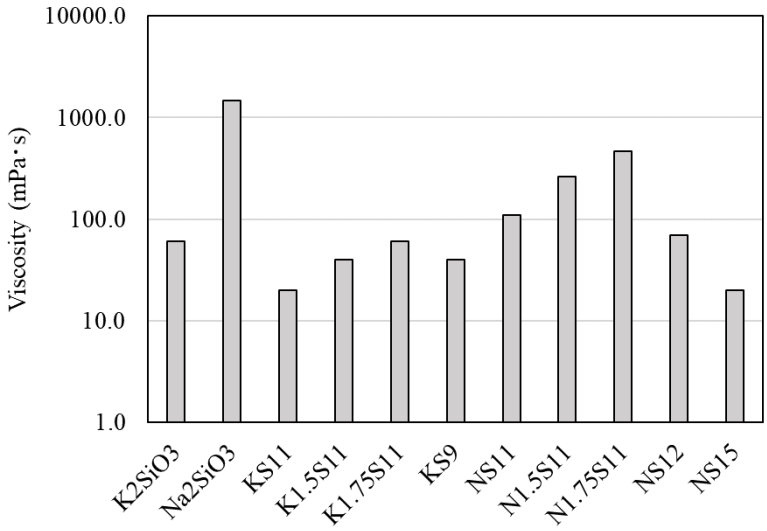

Fig. 3 Viscosities of different alkali activators

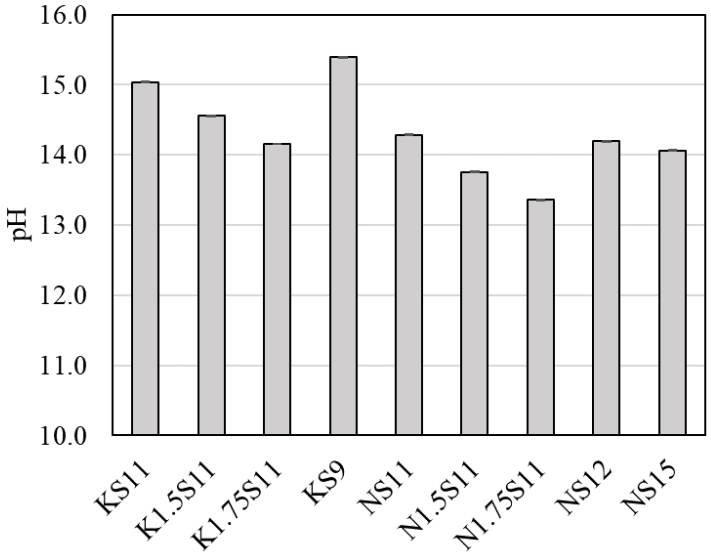

Fig. 4 pH values of different alkali activators

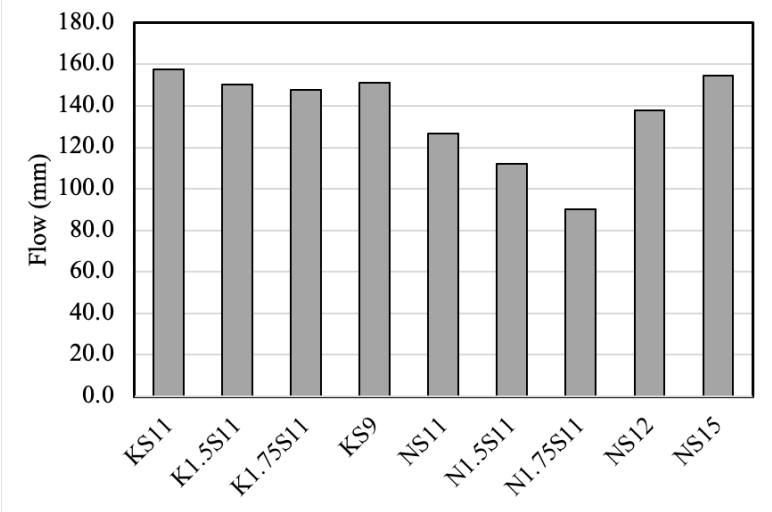

Fig. 5 Flow values of different alkali activators

3.3 Mechanical properties

The uniaxial compressive strength results are presented shown in Fig. 6. For the K-based samples, the strength increased as the SiO_2/Al_2O_3 ratio increased. In addition, the increase in the H_2O/Al_2O_3 ratio resulted in a decrease in strength at 3 day; however, this trend reversed at 28 day, with the increase in the H_2O/Al_2O_3 ratio causing an increase in strength. In contrast, in the Na-based samples, the maximum strength was observed in N1.5S11 at 3 day; however, the strength increased with the SiO_2/Al_2O_3 ratio at 28 day. Specially, N1.75S11 exhibited increased strength of approximately 1.8 times from 3 to 28 day. In the case of the same SiO_2/Al_2O_3 ratio, the strength increased as the H_2O/Al_2O_3 ratio increased. According to Duxson et al., the strength increased with an increasing Si/Al ratio, but no trend was observed for alkali species [25]. Cai et al. and Wang et al. investigated the effects of KOH and NaOH concentrations on strength, respectively. In both cases, an increase in alkaline activator concentration resulted in an increase in strength [19,32]. The strength increased with a decrease in the H_2O/Al_2O_3 ratio because an increase in the pH value of the alkali activator promoted the reaction of geopolymers.

Fig. 7 presents the UPV measurement results. The decrease in H_2O/Al_2O_3 ratio is attributed to the high UPV values. An increase in the SiO_2/Al_2O_3 ratio delayed the UPV being constant.

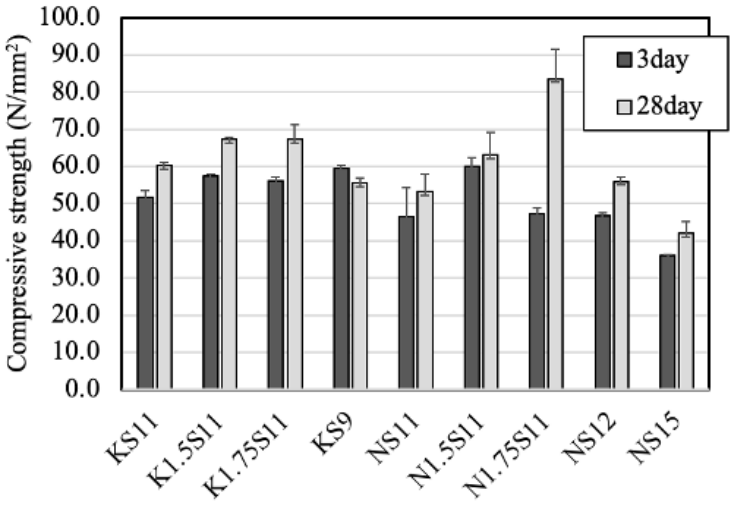

Fig. 6 Compressive strength values at 3 and 28 day

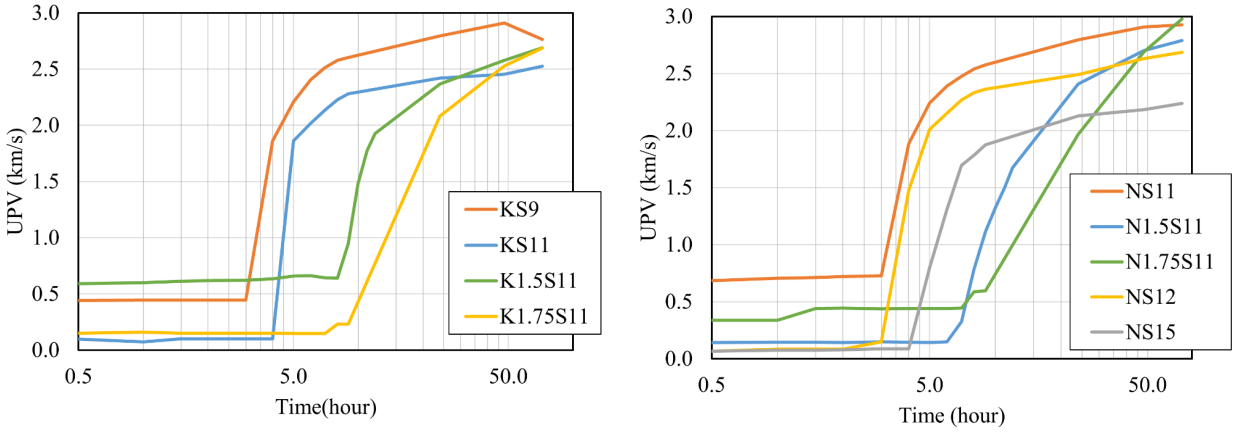

Fig. 7 Variations in UPV with time

3.4 Heat flow

Fig. 8 shows the variations in heat flow with time. When the SiO_2/Al_2O_3 or H_2O/Al_2O_3 ratio was the same, the peak of heat flow was higher for K-based samples than Na-based samples. This may be related to the pH value of the alkali activator and the ease of dehydration during condensation polymerization. When the SiO_2/Al_2O_3 or H_2O/Al_2O_3 ratio was the same, the pH value was higher for K-based solutions than Na-based solutions (Fig. 4). In the case of samples with H_2O/Al_2O_3 = 11, the peak decreased as the SiO_2/Al_2O_3 ratio increased, and the peak time was also delayed. For the samples with SiO_2/Al_2O_3 = 3.0, the peak value decreased as the H_2O/Al_2O_3 ratio increased, except for NS11.

The results for cumulative heat at 3 day are presented in Fig. 9. When the SiO_2/Al_2O_3 or H_2O/Al_2O_3 ratio was the same, similar to the heat flow trend, the cumulative heat was higher for K-based samples than Na-based samples. An increase in the SiO_2/Al_2O_3 ratio suppressed heat generation and promoted the heat evolution after 3 days. For the samples with SiO_2/Al_2O_3 = 3.0, regardless of alkali species or H_2O/Al_2O_3 ratio, the reaction was completed by the third day.

Furthermore, the cumulative heat curves presented in Fig. 10 are closely related to the heat flow characteristics. During heat flow, samples with high peak and early convergence of reactions tended to exhibit significant cumulative heat.

In contrast, delayed reactions showed a decrease in the cumulative heat. Similar trends of heat evolution and cumulative heat were observed by Sun et al. and Liang et al. [16,18]. Sun et al. found that reaction heat slightly increased with decreased liquid-to-solid ratio, which is consistent with the findings of our study because the liquid-to-solid ratio in their study and our H_2O/Al_2O_3 ratio are the same parameter [21]. Liang et al. reported that reaction heat decreased with an increase in SiO_2/Al_2O_3 ratio [16]. According to Rovnanik [22] and Chen et al. [24], these trends may be related to very early dissolution of the precursor. Rapid-polymerization Al^{3+} in metakaolin and Si monomers or oligomers caused that metakaolin particles to become sealed by a layer of geopolymer [22,24]. Therefore, when heat flow showed high peak and early convergence, the cumulative heat decreased. In addition, the heat flow is related to strength, as observed by Albidah et al. Specimens heated and cured at 400 °C had a more porous and sponge-like structure than those cured at room temperature [33]. High heat flow increases porosity and causes cracking, which result in strength reduction.

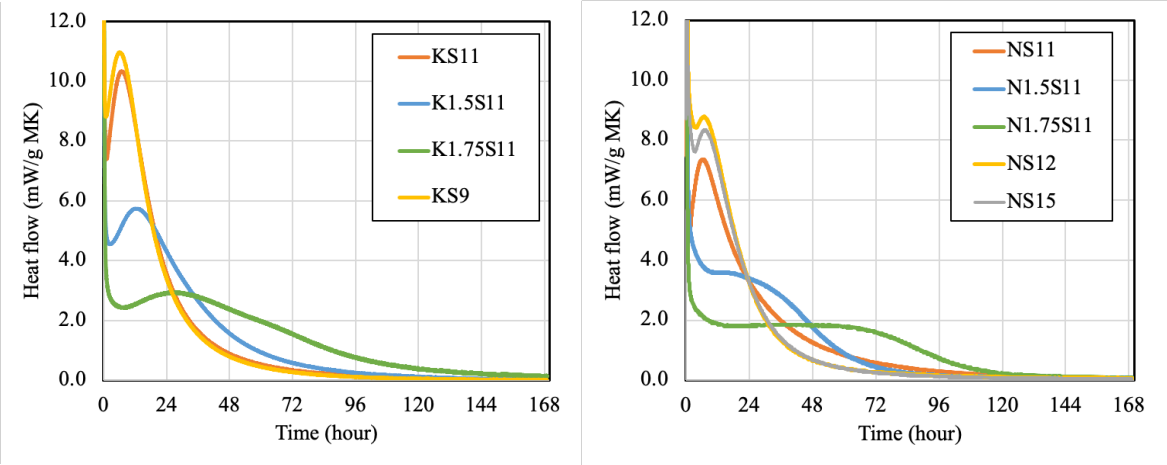

Fig. 8 Variations in heat flow of samples with time

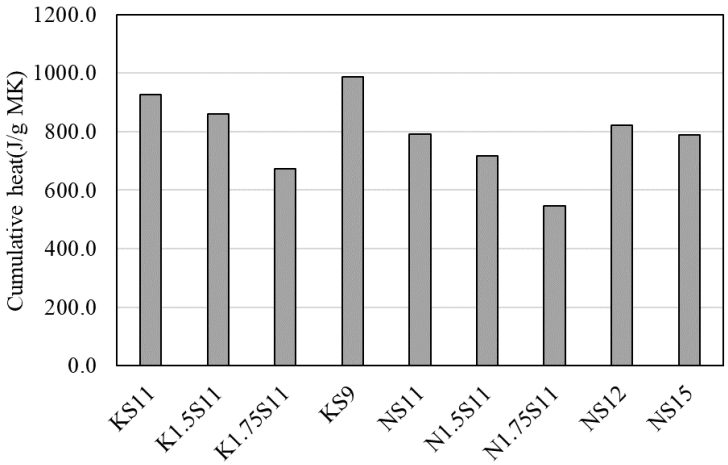

Fig. 9 Cumulative heat values up to 3 day

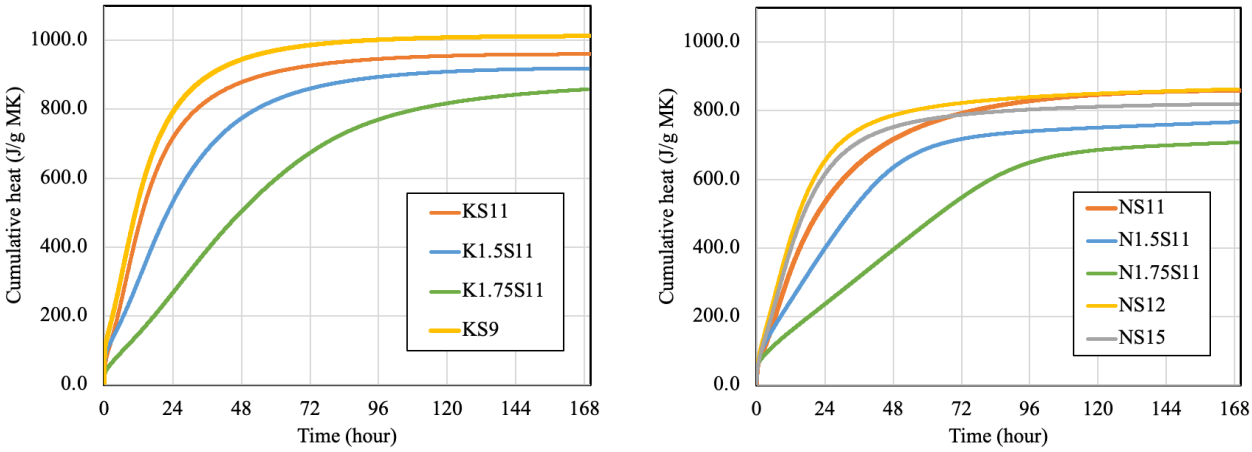

Fig. 10 Variations in cumulative heat of samples with time

Krstulovic et al. proposed a conceptual reaction model of cement hydration [34]. This model is used for crystal-growing systems; however, it has not been extensively used to analyze metakaolin geopolymers, which is amorphous and has a structure similar to that of natural zeolite. Nevertheless, Liu et al. and Fernandez-Jimenez et al. applied this model to geopolymers with blast-furnace slag as the binder and determined the reaction rates [35,36]. Therefore, this model can be used to analyze metakaolin-based geopolymers and their reaction mechanisms.

The model considers three main reaction processes: nucleation and crystal growth (NG), interactions at phase boundaries (I), and diffusion (D). The rate of reaction of each process can be determined from the heat evolution. The Avrami-Erofeev equation, expressed by Eq. (1), describes a reaction dominated by the nucleation and growth processes. In general, the reaction during interactions at phase boundaries are determined using Eq. (2). Eq. (3), proposed by Jander, provides a comprehensive explanation of the diffusion process.

$$[-\ln(1-\alpha)]^{\frac{1}{n}} = K_1 r^{-1}(t-t_0) = K'_1(t-t_0) \quad (1)$$

$$\left[1-(1-\alpha)^{\frac{1}{3}}\right] = K_2 r^{-1}(t-t_0) = K'_2(t-t_0) \quad (2)$$

$$\left[1-(1-\alpha)^{\frac{1}{3}}\right]^2 = K_3 r^{-1}(t-t_0) = K'_3(t-t_0) \quad (3)$$

In Eqs. (1)–(3), α is the degree of reaction, $K_1(K'_1)$, $K_2(K'_2)$, and $K_3(K'_3)$ are rate constants corresponding to NG, I and D, t is the reaction time, t_0(h) is the ending time of the induction period, and n is the crystal growth index within the range, $1 \leqq n \leqq 2$. The crystal growth has the form of needles for $n = 1$ and sheets for $n = 2$.

In Eqs. (1)–(3), α is differentiated by t, and the following equations are derived:

$$\frac{d\alpha}{dt} = F_1(\alpha) = K_1(1-\alpha)[-ln(1-\alpha)]^{\frac{n-1}{n}} \quad (4)$$

$$\frac{d\alpha}{dt} = F_2(\alpha) = 3K_2(1-\alpha)^{\frac{2}{3}} \quad (5)$$

$$\frac{d\alpha}{dt} = F_3(\alpha) = \frac{\frac{3}{2}\left[K_3(1-\alpha)^{\frac{2}{3}}\right]}{\left[1-(1-\alpha)^{\frac{1}{3}}\right]} \quad (6)$$

where $F_1(\alpha)$, $F_2(\alpha)$, and $F_3(\alpha)$ represent each reaction process. The degree of reaction, $\alpha(t)$, and the rate of reaction, $d\alpha/dt$, are defined by Eqs. (7) and (8), respectively.

$$\alpha(t) = \frac{Q'(t)}{Q'max} \quad (7)$$

$$\frac{d\alpha}{dt} = \frac{dQ}{dt} \cdot \frac{1}{Q'max} \quad (8)$$

where Q'(J/g MK) is the cumulative heat at t(h). The cumulative heat Q'_{max} (J/g MK) at the end of the reaction is predicted from the Knudsen extrapolation, as expressed by Eq. (9):

$$\frac{1}{Q'} = \frac{1}{Q'max} + \frac{t_{50}}{Q'\,max(t-t_0)} \quad (9)$$

where t_{50} is the time when samples release 50% of the cumulative heat. Q'max and t_{50} were calculated by plotting 1/Q' and $1/(t-t_0)$ in a line.

Fig. 11showed a fitting curve plotted for KS11. The kinetic parameters were calculated based on this model and the cumulative heat values (Table 3). The maximum heat flow rate (Q'_{max}) was 900 (J/g MK) for most K-based samples. The crystal growth index (*n*) ranged from 1.035 to 1.207, indicating that the dimension of crystal growth remained relatively consistent. An increase in the SiO_2/Al_2O_3 ratio resulted in a decrease in *n* and the promotion of one-dimensional growth. α_1 and α_2 represent the respective degrees of reaction at which the dominant reaction process changes from NG to I, and I to D; however, α_1 was not mostly observed in this study. α_2 increased as the SiO_2/Al_2O_3 ratio increased. t_{50} did not have a trend under this mix condition. According to Liu et al. and Fernandez-Jimenez et al., high values of *n* were obtained and α_1 was observed when the slag reacted with the alkali activator [35,36].

K_1 and K_2 decreased as the SiO_2/Al_2O_3 ratio increased. For Na-based, these values decreased as the H_2O/Al_2O_3 ratio decreased, and a decrease in pH resulted in an increase in the reaction rate. In contrast, the decrease in K_3 with increasing SiO_2/Al_2O_3 ratio was slight compared with those of other rate constants. This suggests that increasing SiO_2/Al_2O_3 ratio suppresses the reaction rate during the early stages; however, the reaction continued slowly for a long time.

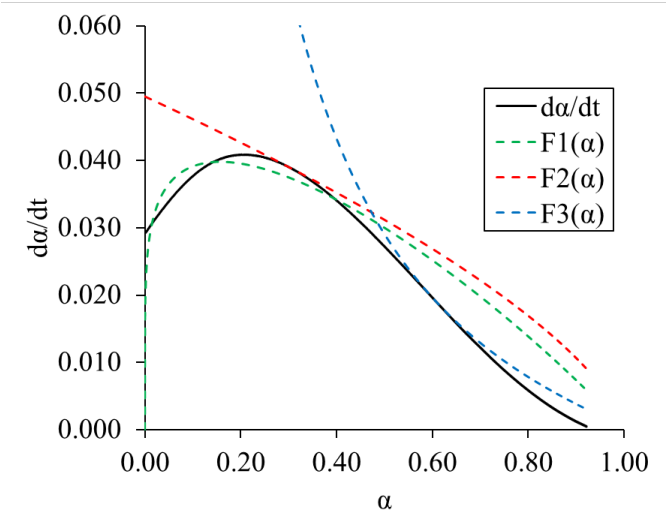

Fig. 11 Plot of fitting of KS11

Table 3 Kinetic parameters determined by the Krstulovic–Davic model

Samples	Q'_{max}	n	K_1	K_2	K_3	α_2	t_{50}
KS11	909.9	1.207	0.0530	0.0165	0.00635	0.483	8.10
K1.5S11	902.5	1.090	0.0246	0.0091	0.00320	0.443	17.38
K1.75S11	885.0	1.069	0.0140	0.0051	0.00267	0.605	22.16
KS9	888.9	1.152	0.0568	0.0178	0.00710	0.487	6.34
NS11	881.1	1.179	0.0387	0.0109	0.00303	0.361	18.59
N1.5S11	593.8	1.059	0.0268	0.0092	0.00508	0.622	13.80
N1.75S11	564.7	1.037	0.0134	0.0066	0.00448	0.712	14.23
NS12	705.2	1.065	0.0549	0.0170	0.00684	0.490	8.06
NS15	706.7	1.094	0.0534	0.0167	0.00709	0.511	6.04

3.5 Degree of reaction and compressive strength

The relationships between the degree of reaction and the compressive strength at 3 and 28 days are discussed. The degree of reaction at 3 day was calculated using Eq. (10):

$$\alpha(3d) = \frac{Q(3d)}{Q'_{max} + Q(t_0)} \times 100 \qquad (10)$$

where $Q(t_0)$ is the cumulative heat at t_0(h). The strength of K-based samples ranged from 50 to 60 N/mm^2, regardless of the degree of reaction, but the Na-based samples had no specific trend (Fig. 12). Differences in the charge density and hydration energies of K and Na are believed to cause the tendency for alkali species, but this was not investigated in this study.

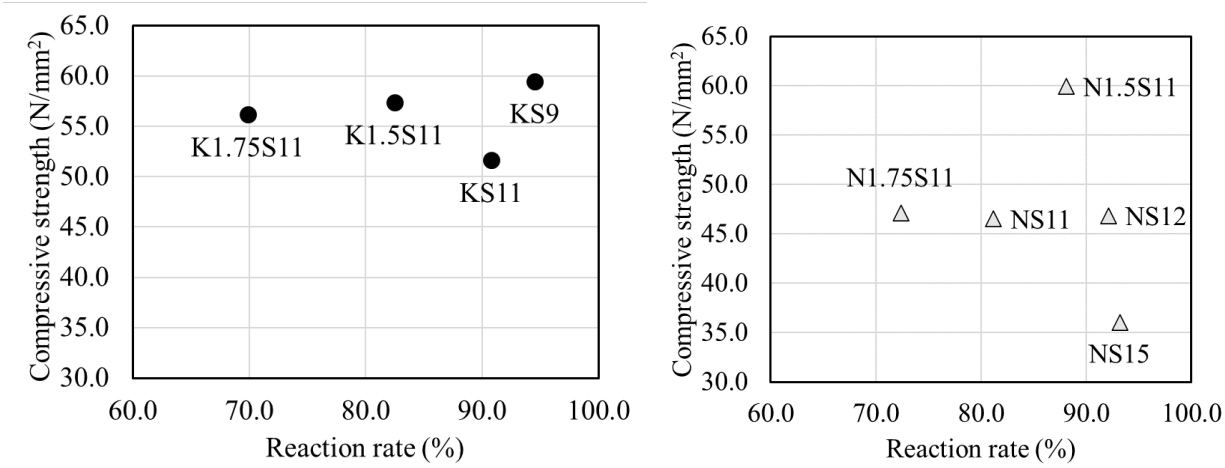

Fig. 12 Plots of compressive strength and degree of reaction

The reaction rate increased with strength, whereas samples with SiO_2/Al_2O_3 = 3.5 showed higher strength than samples with SiO_2/Al_2O_3 = 3.0 and 3.75, regardless of the degree of reaction. According to Duxon et al., unreacted metakaolin may be related to the strength development [37]. Compressive strength increased with increasing Si/Al ratio up to Si/Al = 1.9, but decreased when the Si/Al ratio was increased from 1.9 to 2.15 [25]. Therefore, unreacted metakaolin may be related to the mechanism of higher strength at a lower degree of reaction. However, it is necessary to clarify the amount of unreacted metakaolin.

Compressive strength decreased as the H_2O/Al_2O_3 ratio increased, regardless of alkali species; however the degree of reaction exceeded 90% for most specimens. This may be attributed to excess water, which causes reduction in strength. The increase in the degree of reaction from NS11 to NS12 or NS15 can be explained by the flow test results. For Na-based samples, the value increased as the H_2O/Al_2O_3 ratio increased, and the flowability improved significantly. Therefore, the degrees of reaction of NS12 and NS15 were higher than that of NS11.

Q_{total} was used as the degree of reaction at 28 days to investigate the relationship between the compressive strength and the degree of reaction at 28 days. Q_{total} is expressed as the sum of Q'_{max} and $Q(t_0)$. The relationship between Q_{total} and compressive strength at 28 days is presented in Fig. 13. The Na-based samples showed more variation than the K-based samples and were subject to strength and cumulative heat, depending on the mixing conditions.

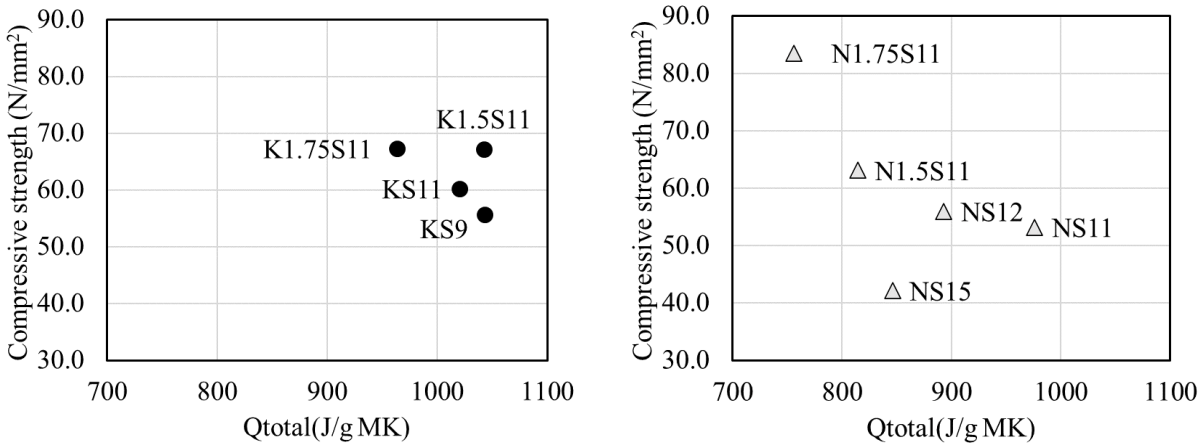

Fig. 13 Plots of compressive strength and Q_{total}

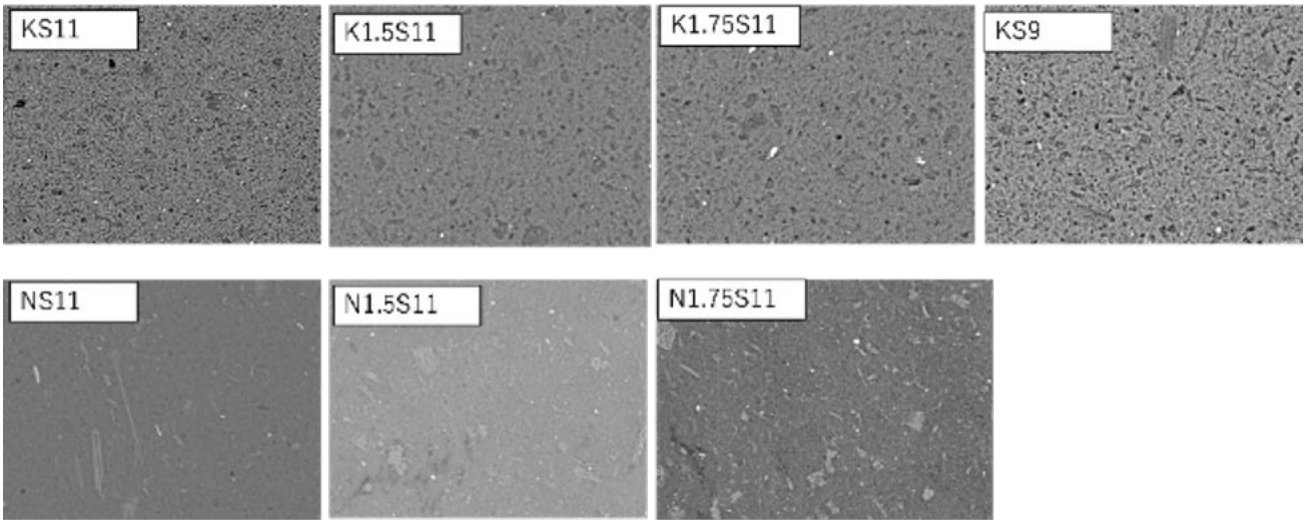

Fig. 14 BSE images of specimens at the 28d (128 μm × 96 μm)

In particular, the cumulative heat of K1.75S11 increased from 3 to 28 day, and the strength increased significantly. For Na-based samples, increasing the SiO_2/Al_2O_3 ratio results in a decrease in the cumulative heat and an increase in the strength. This is because of the presence of unreacted metakaolin, as explained by Duxon et al., but an optimum SiO_2/Al_2O_3 ratio may exist [37]. Fig. 14shows that unreacted metakaolin that remained in this study. The unreacted metakaolin were slightly darker for K-based samples and slightly brighter for Na-based samples. In addition, increasing the SiO_2/Al_2O_3 ratio yielded a brightened area. Brighter areas have a lower density; hence; the unreacted metakaolin affects the strength. Evidence of unreacted metakaolin is shown in supplementary information. The influence of the H_2O/Al_2O_3 ratio on compressive strength indicated that excess water increased porosity and decreased strength. Porosity increases with the $H_2O/(SiO_2+Al_2O_3)$ ratio because excess water evaporates and moves into pores [38].

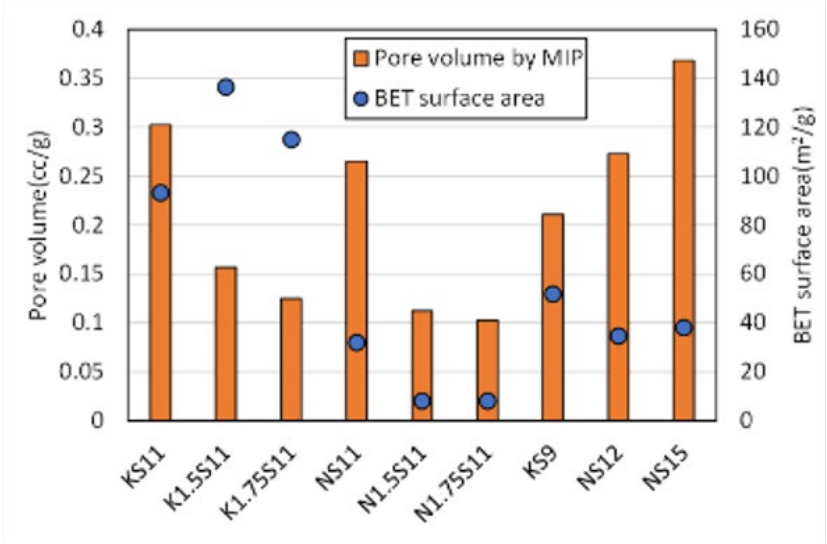

Fig. 15 Porosity measured using MIP and BET surface area at the 28d

3.6 Compressive strength and microstructure

Results for the pore volume and BET surface area are presented in Fig. 15. Porosity tends to decrease as Si/Al increases, and the decrease in the H_2O/Al_2O_3 ratio also decreases the pore volume. Similar trends were obtained for Na-based samples in previous studies [39,40]. The decrease in porosity may result in an increase in fine pores and surface area, but no specific correlation was observed in this study.

The average pore diameters measured using each method are listed in Table 4. Although the absolute values differed, the pore diameters of the K-based samples tended to be smaller and those of the Na-based samples tended to be larger, which was consistent regardless of the measurement method. The increase in the H_2O/Al_2O_3 ratio contributed to the increase in pore size, but no clear trend was observed with respect to the SiO_2/Al_2O_3 ratio. These were also similar to the findings of a previous study [40].

Fig. 16 shows the total correlation function of metakaolin geopolymer at 28 days. The K- and Na-based results differed, including peaks at 2–2.5 Å. This is probably attributed to Na-O bonding in Na-based samples, and the results are similar to those of previous studies on bonding distances, such as Si-O and Al-O [41,42]. The effect of the alkaline activators of Si/Al and H_2O/Al_2O_3 were minimal. The results are consistent with those of solid-state nuclear magnetic resonance measurements from previous studies by the authors [27].

Fig. 17 shows the TEM images. Similar to findings of previous studies, the K-based samples showed solids with a regular shape, whereas the Na-based samples did not show a clear solid shape [43-46]. Circular voids were clearly identified in the Na-based sample. Therefore, the formation of pores differs between Na- and K-based samples. No effect of the H_2O/Al_2O_3 and SiO_2/Al_2O_3 ratios was observed for the same alkali with respect to pore size and shape.

Fig. 18 (a) shows the relationship between the pore volumes measured using MIP and compressive strength. The strength linearly decreased with increasing porosity, indicating that porosity is the main determinant of strength. Although many previous studies have examined differences in water content and the SiO_2/Al_2O_3 ratio [45-47], this study also observed differences in alkali species and a good correlation between porosity and strength. As shown in Figs. 12 and 13, the degree of reaction does not provide a consistent relationship to strength, but the pore volume allows for a more consistent

evaluation. However, because the reaction is the main cause of pore structure formation (Fig. 18(b)), the pore volume increases as the degree of reaction increases, a trend that is different from the reaction of cement. This is attributed to the formation of the pore structure via polycondensation reaction [17,48,49], which is different from the reaction of cement. Hence, microporosity within a few nanopores increases with the reaction [44]. Therefore, it is necessary to clarify the reaction and pore structure formation in the future. Compressive strength (CS) is estimated from the mix proportion via multiple regression analysis and can be expressed by the following equation:

$$CS[N/mm^2] = -4.78AS + 16.6\frac{S}{A} - 3.6\frac{H}{A} + 0.25Age + 72.1 \quad (11)$$

where AS is the alkali species of activator (K:1 or Na:0), S/A is the SiO_2/Al_2O_3 ratio of the alkali activator, H/A is the H_2O/Al_2O_3 of the alkali activator, Age is the curing age (day). This equation enables estimation with an error of 20%, as shown in Fig. 18(c). The SiO_2/Al_2O_3 ratio was found to be the most important contributor to strength development. The alkali species, being K-based, may not have a positive effect on strength development because excessive reaction leads to the loss of unreacted metakaolin. As this study was conducted using a type of metakaolin with good reactivity, K-based alkalis may be effective for less reactive metakaolin.

Table 4 Pore sizes measured using MIP, NAD and SAXS at 28d

	Average pore size by MIP (nm)	**Average pore size by N_2 adsorption(nm)**	**Pore diameter measured by SAXS(nm)**
KS11	5.65	8.90±0.5	16.4±0.01
K1.5S11	6.25	6.36±2.9	11.3±0.02
K1.75S11	6.34	10.5±5.5	-
KS9	5.57	16.8±9.0	15.2±0.01
NS11	12.8	24.2±4.5	22.5±0.02
N1.5S11	7.09	29.0±4.6	-
N1.75S11	7.38	29.5±5.1	-
NS12	13.4	22.7±0.4	-
NS15	23.5	27.9±1.2	-

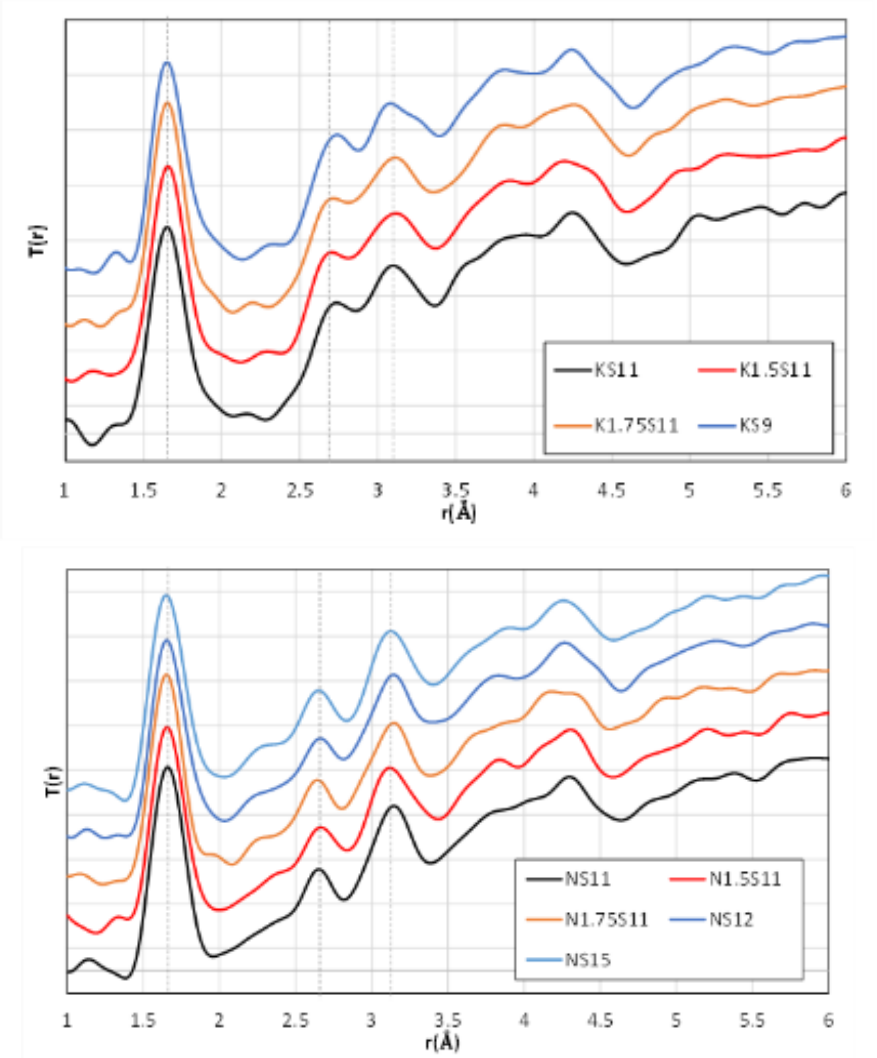

Fig. 16 Total correlation functions of metakaolin geopolymer at 28d

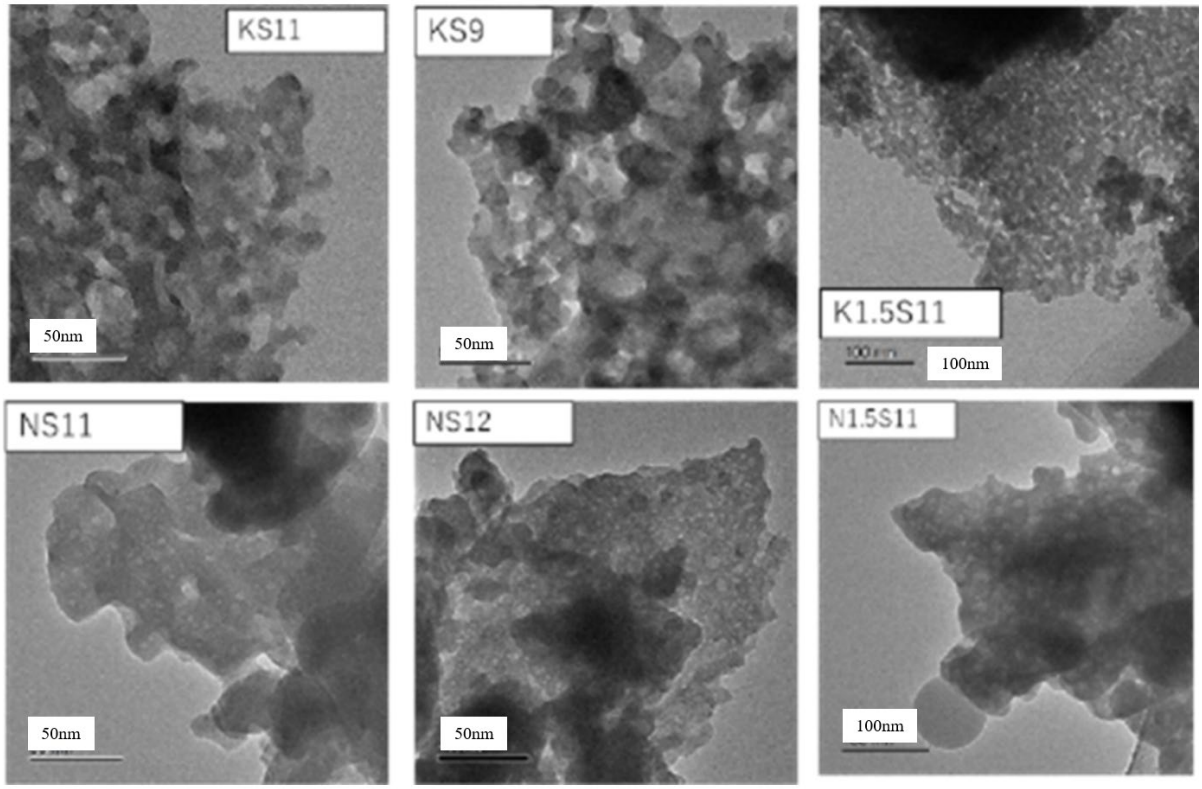

Fig. 17 TEM observations of geopolymer at 28d

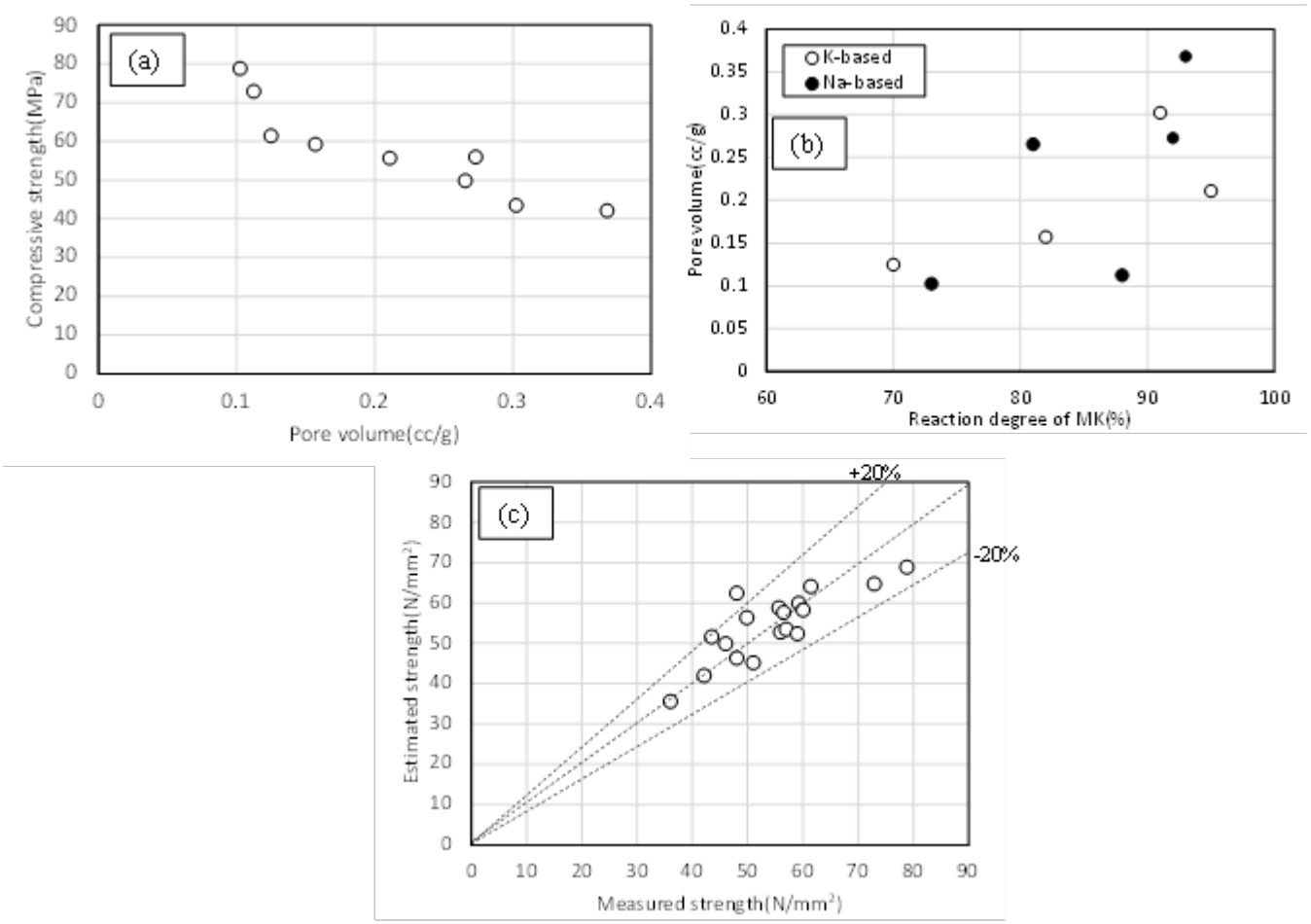

Fig. 18 Plots of (a) pore volume measured using MIP and compressive strength, (b) pore volume measured using MIP and the degree of reaction of metakaolin, and (c) measured strength and strength estimated using Eq. (11)

4. Conclusion

In this study, the initial reaction of metakaolin geopolymer was investigated, and the heat of reaction was measured using a calorimeter. Several methods were applied to clarify changes in the microstructure. The following conclusions were drawn.

1). The viscosity of alkali activators is influenced by the mix proportion. The Na-based solutions had higher viscosity values than the K-based solutions. Furthermore, higher viscosity was obtained for higher SiO_2/Al_2O_3 ratios and lower H_2O/Al_2O_3 ratios. The trend of viscosity determined by mix proportion was consistent with that of the flow results. The pH of alkali activators increased when alkali species is Ka and the SiO_2/Al_2O_3 and H_2O/Al_2O_3 ratios are low.

2). Compressive strength at 3 days reached 80% of that at 28 days, except for N1.75S11. The strength was determined by the reaction up to the third day. Higher UPV values were obtained for lower H_2O/Al_2O_3 ratios. A higher SiO_2/Al_2O_3 ratio delayed the UPV in being constant.

3). Cumulative heat indicated the degree of reaction and was characterized using calorimeter measurements. Heat flow with high peak and early convergence of reactions tended to yield high cumulative heat. This tendency was observed for samples with low SiO_2/Al_2O_3 and H_2O/Al_2O_3 ratios.

4). The trend of the reaction rate was quantitatively analyzed using the Krstulovic-Davic model. K_1, K_2 and K_3 of the kinetic parameters determined the value of each reaction rate. Samples with lower SiO_2/Al_2O_3 and H_2O/Al_2O_3 ratios continued to react slowly for a longer time than those with higher ratios. These yielded decerased K_1 and K_2 and increased K_3. Furthermore, these constants were featured by mix design relating to workability and pH. Increasing the SiO_2/Al_2O_3 ratio and decreasing the H_2O/Al_2O_3 ratio resulted in low flow and pH values.

5). From the relationship between compressive strength and cumulative heat, it was assumed that a certain degree of reaction progression and the presence of unreacted metakaolin were necessary for strength increase. Increasing the H_2O/Al_2O_3 ratio resulted in increasing pore volume and decreasing strength. Therefore, the optimal mix proportion for higher strength at 28 days is SiO_2/Al_2O_3 = 3.5 or 3.75 and H_2O/Al_2O_3 = 11 in K-based. In Na-based, the proportion is SiO_2/Al_2O_3 = 3.75 and H_2O/Al_2O_3 = 11 or 12. This is because it affects the formation of the pore structure, and different alkalis have a significant effect on the formation of pore structure and resultant strength development.

6). An equation for estimating the compressive strength from the mix proportion and curing age was determined by multiple regression analysis, showing that the strength can be estimated with an error of about 20%. The amount of alkali species could not be quantified in this study. Therefore, the Na_2O/Al_2O_3 and K_2O/Al_2O_3 ratios should be varied to estimate this effect in future studies.

Acknowledgment: This study was partially supported by The Taisei Foundation and JSPS KAKENHI Grant Number 24K07745. Mr. Nakamura polished the samples, and Mr. Ota assisted in the TEM measurements. The synchrotron radiation experiments were performed at the BL04B2 of SPring-8 with the approval of the Japan Synchrotron Radiation Research Institute (JASRI) (Proposal No. 2024B1092). We hereby express our gratitude.

CRediT author statement:

K.Kurumisawa: Conceptualization, Methodology, Writing—Reviewing and Editing, Investigation, Supervision, Funding acquisition

H.Nakashima: Data curation, Writing—Original draft preparation, Investigation.

Supplementary information

Al is concentrated in areas where K and Na not present. Al-rich area shows that unreacted metakaolin is present. In original images, unreacted metakaolin is present in brighter areas.

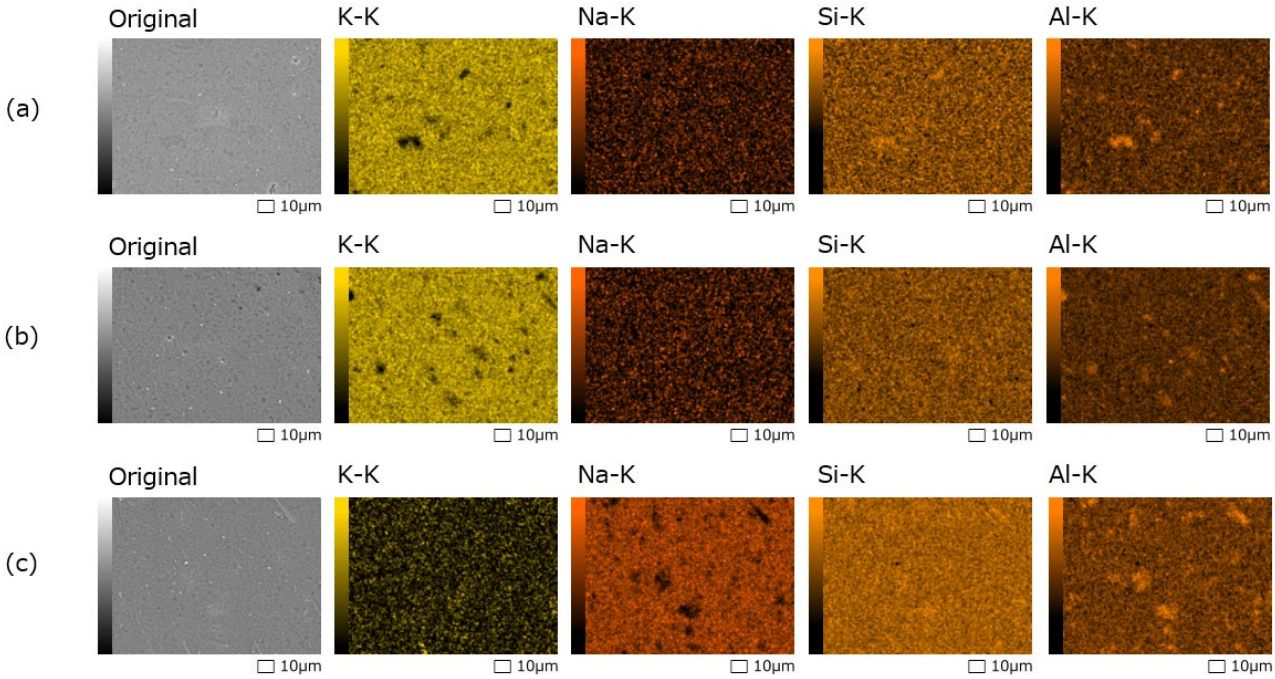

Fig.S19 SEM-EDX Images (a)KS11, (b)KS9, (c) NS11 at 28d

References

[1] Benhelal E, Shamsaei E, Rashid MI. Challenges against CO2 abatement strategies in ce ment industry: A review. Journal of Environmental Sciences. 2021 June;104:84-101.

[2] Supriya, Chaudhury R, Sharma U, Thapliyal PC, Singh LP. Low-CO2 emission strategies to achieve net zero target in cement sector. Journal of Cleaner Production. 2023 Sep 1 0;417:137466.

[3] Davidovits J. GEOPOLYMRS AND GEOPOLYMRIC MATERIALS. Journal of Thermal Analysis. 1989 Mar;35:429-441.

[4] Chakkor O, Altan MF, Canpolat O. Elevated Temperature, Freezing–Thawing and Mechanical Properties of Limestone, Marble, and Basalt Powders Reinforced Metakaolin–Red Mud-Based Geopolymer Mortars. Iranian Journal of Science and Technology, Transactions of Civil Engineering. 2022 Aug;46(4):3241-3258

[5] Harada K. Geopolymer, a new material that is friendly to nature. Land improvement. 2016 Apr;293:67-69.

[6] Temuujin J, Minjigmaa A, Rickard W, Lee M, Williams I, Riessen A. Preparation of metakaolin based geopolymer coatings on metal substrates as thermal barriers. Applied Clay Science. 2009 Nov;46(3): 265–270.

[7] Bouguermouh K, Bouzidi N, Mahtout L, Villarejo LP, Martínez-Cartas ML. Effect of aci d attack on microstructure and composition of metakaolin-based geopolymers: The role o f alkaline activator. 2017 May;463:128-137.
[8] Japan Concrete Inst. Report of the Research Committee on the Application of Geopolymer Technology to the Construction Field. 2017
[9] Zhang B. Durability of low-carbon geopolymer concrete: A critical review. Sustainable Materials and Technologies. 2024 July;40:e00882
[10] Zhang B, Zhu H, Cheng Y, Huseien GF, Shah KW. Shrinkage mechanisms and shrinkage-mitigating strategies of alkali-activated slag composites: A critical review. Construction and Building Materials. Feb;318:125993
[11] Haddad MA, Harnik Y, Schlosser Y, Goldbourt A. Cesium immobilization in metakaolin-based geopolymers elucidated by 133Cs solid state NMR spectroscopy. Journal of Nuclea r Materials. 2022 Apr 15;562:153570.
[12] López FJ, Sugita S, Tagaya M, Kobayashi T. Metakaolin-Based Geopolymers for Targete d Adsorbents to Heavy Metal Ion Separation. Journal of Materials Science and Chemical Engineering. 2014 July;7(2):16-27.
[13] Trincal V, Multon S, Benavent V, Lahalle H, Balsamo B, Caron A, Bucher R, Caselles LD, Cyr M. Shrinkage mitigation of metakaolin-based geopolymer activated by sodium silicate solution. Cement and Concrete Research. 2022 Dec;162:106993.
[14] Kani EN, Allahverdi A, Provis JL. Efflorescence control in geopolymer binders based on natural pozzolan. Cement and Concrete Composites. 2012 Jan;34(1):25-33.
[15] Ichimiya K, Hatanaka S, Atarashi D. Current State and Future Prospects of Geopolymer s. Concrete Engineering. 2018;56(5):409-414.
[16] Liang G, Yao W, She A. New insights into the early-age reaction kinetics of metakaolin geopolymer by 1H low-field NMR and isothermal calorimetry. Cement and Concrete Co mposites. 2023; 137: 104932.
[17] Gharzouni A, Joussein E, Samet B, Baklouti S, Rossignol S. Effect of the reactivity of alkaline solution and metakaolin on geopolymer formation. Journal of Non-Crystalline So lids. 2015 Feb 15;410:127–134.
[18] Sun Z, Vollpracht A. Isothermal calorimetry and in-situ XRD study of the NaOH activat ed fly ash, metakaolin and slag. Cement and Concrete Research. 2018 Jan;103:110-122.
[19] Cai J, Li X, Tan J, Vandevyvere B. Thermal and compressive behaviors of fly ash and metakaolin-based geopolymer. Journal of Building Engineering. 2020 July;30:101307.
[20] Dupuy C, Havette J, Gharzouni A, Texier-Mandoki N, Bourbon X, Rossignol S. Metaka olin-based geopolymer: Formation of new phases influencing the setting time with the us e of additives. Construction and Building Materials. 2019 May;200: 272-281.
[21] Lizcano M, Kim HS, Basu S, Radovic M. Mechanical properties of sodium and potassiu m activated metakaolin-based geopolymers. J Mater Sci. 2012 May;47(6):2607-2616.
[22] Rovnaník P. Effect of curing temperature on the development of hard structure of metak aolin-based geopolymer. Construction and Building Materials. 2010;24(7):1176–1183.
[23] Zuhua Z, Xiao Y, Huajun Z, Yue C. Role of water in the synthesis of calcined kaolin-based geopolymer. Applied Clay Science. 2009 Feb;43(2):218–223.

[24] Chen L, Wang Z, Wang Y, Feng J. Preparation and Properties of Alkali Activated Meta kaolin-Based Geopolymer. Materials. 2016;9(9):767.
[25] Duxson P, Mallicoat SW, Lukey GC, Kriven WM, Van Deventer JSJ. The effect of alkal i and Si/Al ratio on the development of mechanical properties of metakaolin-based geop olymers. Colloids and Surfaces A: Physicochem. Eng. Aspects. 2007 Jan;292(1):8–20.
[26] Sasaki K, Kurumisawa K, Ibayashi K. Effect of retarders on flow and strength developm ent of alkali-activated fly ash/blast furnace slag composite. Constr. Build. Mater. 2009 A ug 20;216:337-346.
[27] Kurumisawa K, Omatu H, Yamashina Y. Effect of alkali activators on diffusivity of met akaolin-based geopolymers. Mater. Struct. 2021 Aug 6;54:169.
[28] Oliveira MF, Lameiras FS. Mix design formulation range for metakaolin-based geopolym er synthesis. Metallurgy and materials REM, Int. Eng. J. 2022;75(3):225-234.
[29] Kohara S, Itou M, Suzuya K, Inamura Y, Sakurai Y, Onishi Y, Takata M. Structural studies of disordered materials using high-energy x-ray diffraction from ambient to extreme conditions. Journal of Physics: Condensed Matter. 2007 Nov 8;19(50):506101.
[30] Jansson H, Bernin D, Ramser K. Silicate species of water glass and insights for alkali-a ctivated green cement. AIP ADVANCES 2015 June 1;5(6):067167 .
[31] Jiang T, Liu Z, Tian X, Wu J, Wang L. Review on the impact of metakaolin-based geo polymer's reaction chemistry, nanostructure and factors on its properties. Construction an d Building Materials. 2024;412:134760.
[32] Wang H, Li H, Yan F. Synthesis and mechanical properties of metakaolinite-based geopo lymer. Colloids and Surfaces A: Physicochem. Eng. Aspects. 2005 Oct;268(1-3): 1–6 .
[33] Albidah A, Alqarni AS, Abbas H, Almusallam T, Al-Salloum Y. Behavior of Metakaolin -Based geopolymer concrete at ambient and elevated temperatures. Construction and Buil ding Materials. 2022 Jan 24;317:125910.
[34] Krstulović R, Dabić P. A conceptual model of the cement hydration process. Cement an d Concrete Research. 2000 May;30(5):693-698.
[35] Liu S, Li Q, Han W. Effect of various alkalis on hydration properties of alkali-activated slag cements. J Therm Anal Calorim. 2018 Mar;131(3):3093–3104.
[36] Fernández-Jiménez A, Puertas F, Arteaga Á. DETERMINATION OF KINETIC EQUATI ONS OF ALKALINE ACTIVATION OF BLAST FURNACE SLAG BY MEANS OF C ALORIMETRIC DATA. Journal of Thermal Analysis, 1998 June 1;52(3):945-955.
[37] Duxson, P., Provis, J. L., Lukey, G. C., Mallicoat, S. W., Kriven, W. M., van Deventer, J. S. J., (2005). "Understanding the relationship between geopolymer composition, micros tructure and mechanical properties." Colloids and Surfaces A: Physicochem. Eng. Aspects 269, 47–58
[38] Lizcano M, Gonzalez A, Basu S, Lozano K, Radovic M. Effects of Water Content and Chemical Composition on StructuralProperties of Alkaline Activated Metakaolin-Based Geopolymers. J. Am. Ceram. Soc. 2012 Apr 10;95(7):2169–2177
[39] Benavent, V., Frizon, F., Poulesquen, A., (2016). "Effect of composition and aging on the porous structure of metakaolin-based geopolymers." Journal of Applied Crystallography 49. 6: 2116-2128.

[40] Pouhet R, Cyr M, Bucher R. Influence of the initial water content in flash calcined metakaolin-based geopolymer. Construction and Building Materials. 2019 Mar 20;201:421-429
[41] White CE, Page K, Henson NJ, Provis JL. In situ synchrotron X-ray pair distribution function analysis of the early stages of gel formation in metakaolin-based geopolymers. Applied Clay Science. 2013 Mar;73:17-25.
[42] White CE, Provis JL, Proffen T, Van Deventer JSJ. The effects of temperature on the local structure of metakaolin-based geopolymer binder: A neutron pair distribution function investigation. Journal of the American Ceramic Society. 2010 July 15;93(10):3486-3492.
[43] Autef A, Joussein E, Gasgnier G, Pronier S, Sobrados I, Sanz J, Rossignol S. Role of metakaolin dehydroxylation in geopolymer synthesis. Powder technology. 2013 Dec;250:33-39.
[44] Bell JL, Driemeyer PE, Kriven WM. Formation of ceramics from metakaolin-based geopolymers. Part II: K-based geopolymer. *Journal of the American Ceramic Society.* 2009 Mar 16;92(3):607-615.
[45] Matiland CF, Buckley CE, O'Connor BH, Butler PD, Hart RD. Characterization of the pore structure of metakaolin-derived geopolymers by neutron scattering and electron microscopy. Journal of Applied Crystallography. 2011 Aug 1;44(4):697-707
[46] Duxson P, Provis JL, Lukey GC, Mallicoat SW, Kriven WM, Van Deventer JSJ. Understanding the relationship between geopolymer composition, microstructure and mechanical properties. Colloids and Surfaces A: Physicochemical and Engineering Aspects. 2005 Nov;269(1-3):47-58
[47] Yan D, Xie L, Qian X, Ruan S, Zeng Q. Compositional dependence of pore structure, strength and freezing-thawing resistance of metakaolin-based geopolymers. *Materials* 2020 July 3;13(13):2973.
[48] Frederickx L, Nguyen TN, Phung QT. Strength and microstructure characteristics of metakaolin-based geopolymer mortars with high water-to-binder ratios. Sustainability. 2022 Mar 8;14(6):3141.
[49] Peng H, Yang Y, Ge Y, Li Y, Shi XFASCE. Metakaolin-based geopolymer features different pore structure characteristics from ordinary portland cement paste: a mechanistic study. Journal of Materials in Civil Engineering. 2022 Sep 19;34(12):04022321.
[50] Wan Q, Rao F, Song S, García RE, Estrella RM, Patiño CL, Zhang Y. Geopolymerization reaction, microstructure and simulation of metakaolin-based geopolymers at extended Si/Al ratios. Cement and Concrete Composites. 2017 May;79:45-52.
[51] Autef A, Joussein E, Poulesquen A, Gasgnier G, Pronier S, Sobrados I, Sanz J, Rossignol S. Influence of metakaolin purities on potassium geopolymer formulation: the existence of several networks. *Journal of colloid and interface science.* 2013 Oct 15;408:43-53.
[52] Barbosa VFF, MacKenzie KJD, Thaumaturgo C. Synthesis and characterisation of materials based on inorganic polymers of alumina and silica: sodium polysialate polymers. International Journal of Inorganic Materials. 2000 Sep;2(4):309–317.
[53] Raphaëlle P, Martin C, Raphaël B. Influence of the initial water content in flash calcined metakaolin-based geopolymer. *Construction and Building Materials.* 2019 Mar 20;201: 421-429.
[54] Shilar FA, Ganachari SV, Patil VB, Nisar KS. Evaluation of structural performances of metakaolin based geopolymer concrete. Journal of Materials Research and Technology. 20 22;20:3208-3228.

[55] Singh NB, Middendorf B. Geopolymers as an alternative to Portland cement: An overvie w. Construction and Building Materials. 2020 Mar 20;237:117455.
[56] Svenum IH, Ringdalen IG, Bleken FL, Höche D, Swang O. Structure, hydration, and chl oride ingress in C-S-H: Insight from DFT calculations. Cement and Concrete Research. 2020 Mar;129:105965.